MOLECULAR PHYSICS, 20 JANUARY 2004, VOL. 102, NO. 2, 223–234

Taylor & Francis
Taylor & Francis Group

Freezing/melting behaviour within carbon nanotubes

FRANCISCO R. HUNG[1], GRAZYNA DUDZIAK[2],
MALGORZATA SLIWINSKA-BARTKOWIAK[2] and KEITH E. GUBBINS[1]*

[1]Department of Chemical Engineering, North Carolina State University,
Raleigh, NC 27695-7905, USA, [2]Institute of Physics, Adam Mickiewicz University,
Umultowska 85, 61-614 Poznan, Poland

(*Received 6 July 2003; revised version accepted 1 December 2003*)

We report a study of the freezing and melting of fluids confined within multi-walled carbon nanotubes with an internal diameter of 5 nm, using experimental measurements and molecular simulations. Dielectric relaxation spectroscopy was used to determine the experimental melting points and relaxation times of nitrobenzene and carbon tetrachloride within carbon nanotubes, and parallel tempering Monte Carlo simulations in the grand canonical ensemble were performed for confined carbon tetrachloride. The simulations show that the adsorbate forms concentric layers that solidify into quasi-two-dimensional hexagonal crystals with defects; highly defective microcrystalline regions are formed in the inner layers, owing to the strong geometrical constraints. Our simulations show no formation of common three-dimensional crystalline structures (fcc, hcp, bcc, sc or icosahedral) in confinement. The results suggest the presence of inhomogeneous phases (i.e., combinations of crystalline and liquid regions) within the pore over extended temperature ranges. Our results indicate that the outer layers of adsorbate solidify at temperatures slightly higher than the bulk freezing point, whereas the inner layers freeze at lower temperatures. The simulation results are in good agreement with the experimental measurements.

1. Introduction

An understanding of freezing phenomena for fluids confined within porous materials is important in the fabrication of nano-structured materials, nanotribology, adhesion, and characterization of porous materials. Studies of these phenomena are, however, plagued by several difficulties. Experimental research is complicated by the lack of well-characterized porous materials with appropriate pore sizes, ambiguities in attempting to determine the nature of the confined phase, and the prevalence of long-lived metastable states. Molecular simulation studies do not suffer from any of these difficulties; moreover, it is possible to determine the free energies of the confined phases, and thus identify the true thermodynamic equilibrium states and the order of the phase transitions. Nevertheless, simulations face other difficulties, such as uncertainties in intermolecular potentials and pore characterization, as well as limitations due to the speed of current supercomputers. The difficulties found in experiments and simulations make the two approaches complementary, so that combined experimental–simulation studies can be rewarding.

Recent studies for pores of simple geometry have shown a complex phase behaviour associated with freezing in confined systems [1–31]. The freezing temperature may be lowered or raised relative to the bulk freezing temperature, depending on the nature of the adsorbate and the porous material. In addition, new surface-driven phases may intervene between the liquid and solid phases in the pore. 'Contact layer' phases of various kinds often occur, in which the layer of adsorbed molecules adjacent to the pore wall has a different structure from that of the adsorbate molecules in the interior of the pore. These contact layer phases have been predicted theoretically and confirmed experimentally for several systems [7, 12, 21]. In addition, for some systems in which strong layering of the adsorbate occurs (e.g., activated carbon fibres), hexatic phases may appear. Such phases are quasi-two-dimensional systems with quasi-long-ranged orientational order, but positional disorder, and were found to be stable over a temperature range between those for the crystal and liquid phases. Hexatic phases have been clearly seen in molecular simulations [21, 22], and recent experiments have provided convincing evidence for them [22]. It has been shown that this apparently complex phase behaviour results from a competition between the fluid–wall

*Author for correspondence. e-mail: keg@ncsu.edu

Molecular Physics ISSN 0026–8976 print/ISSN 1362–3028 online © 2004 Taylor & Francis Ltd
http://www.tandf.co.uk/journals
DOI: 10.1080/00268970410001670090

and fluid–fluid intermolecular interactions. For a given pore geometry and width, the phase diagrams for a wide range of adsorbates and porous solids can be classified in terms of a parameter α that is the ratio of the fluid–wall to fluid–fluid attractive interaction [21].

In this paper we report experimental and molecular simulation studies of freezing within multi-walled carbon nanotubes with an internal diameter of 5 nm. Experimental results from dielectric relaxation spectroscopy are reported for both nitrobenzene and carbon tetrachloride (CCl_4) in carbon nanotubes, and the simulations are for carbon tetrachloride within the same porous material. The experimental and simulation methods are described in § 2. Section 3.1 contains our experimental results, and the simulations are discussed and compared with the experiments in § 3.2. Finally, our conclusions and some suggestions for future work are presented in § 4.

2. Methods

2.1. *Experiment*

The multi-walled carbon nanotube samples were synthesized at CNRS-Orléans through the catalytic decomposition of acetylene at 600°C on a $Co_xMg_{(1-x)}O$ solid solution [32]. The resulting nanotubes were purified in boiling concentrated HCl and their tips opened by treatment with CO_2. The carbon nanotube samples were characterized by TEM and SEM imaging, as well as nitrogen adsorption measurements. The multi-walled carbon nanotubes had seven molecular layers on average, and a narrow pore size distribution, with average internal and external diameters of 5 and 10 nm, respectively. The nitrobenzene and carbon tetrachloride samples were reagent grade chemicals and were distilled twice at reduced pressure before their use in experiments. The nitrobenzene was further dried over Al_2O_3, centrifuged and stored in the absence of light to avoid contamination by photochemical reactions. The carbon nanotube samples were kept under vacuum (10^{-3} torr) and heated to 120°C to remove traces of air and moisture prior to and during the introduction of the fluid samples.

The experimental setup consisted of a parallel plate capacitor of empty capacitance $C_0 = 4.2$ pF. The capacitance, C and the tangent loss, $\tan(\delta)$ (where δ is the angle by which current leads the voltage) of the capacitor filled with the sample were measured at different temperatures using a Solartron 1260 gain impedance analyser in the frequency range 1 Hz–10 MHz. The complex dielectric permittivity $\kappa^* = \kappa_r - i\kappa_i$ is related to the measured quantities by $\kappa_r = C/C_0$, $\kappa_i = \tan(\delta)/\kappa_r$ [7]. As a solid phase sample is heated, phase changes such as melting manifest themselves by a large increase in the permittivity. The melting temperatures for pure nitrobenzene and CCl_4 were determined to be 5.7°C (278.9 K) and −22.9°C (250.3 K), respectively. For fluids confined within carbon nanotubes, the sample was introduced between the capacitor plates as a suspension of adsorbate-filled carbon nanotubes in the pure adsorbate. The measurement thus yields an effective permittivity for the sample. The dielectric, orientational (rotational) relaxation time τ can be obtained from the experimental data using the Debye dispersion relation, which was derived for an isolated dipole rotating under an oscillating electric field in a viscous medium using classical mechanics [33]:

$$\kappa^* = \kappa_{\infty,r} + \frac{\kappa_{s,r} - \kappa_{\infty,r}}{1 + i\omega\tau}. \quad (1)$$

Here, ω is the frequency and the subscript s refers to the static permittivity in the low frequency limit, where the dipoles have enough time to be in phase with the applied field. The subscript ∞ refers to the optical permittivity in the high frequency limit, and is a measure of the induced component of the permittivity. The dielectric relaxation time was obtained by fitting the dispersion spectrum of the complex permittivity (i.e., κ_r and κ_i versus ω) near resonance to the Debye model. The resonant frequencies of the dielectric relaxation in the solid and glass phases were expected to be within the frequency range used in this study. From equation (1), κ_r goes through an inflection point and κ_i shows a maximum at the resonant frequency. As a consequence, from a spectrum plot of κ_r, κ_i versus ω at a fixed temperature, the relaxation time τ can be determined at each temperature as the inverse of the frequency that corresponds to a saddle point of κ_r and a maximum in κ_i. Further details of these experimental methods are described elsewhere [7, 34].

2.2. *Simulation*

The interaction between the adsorbed CCl_4 molecules was modelled using the Lennard-Jones (LJ) (12, 6) potential, with parameters fitted [21] to reproduce the bulk freezing point of CCl_4: $\sigma_{ff} = 0.514$ nm, $\varepsilon_{ff}/k_B = 366.0$ K. The LJ potential was cut off at a distance of $5\sigma_{ff}$. The multi-walled carbon nanotube was modelled as a structureless, cylindrical pore surrounded by a semi-infinite solid [35]. The potential parameters for the carbon nanotube were chosen to be equal to those of graphite [36, 37]: $\rho_w = 114\,\text{nm}^{-3}$, $\sigma_{ww} = 0.340$ nm and $\varepsilon_{ww}/k_B = 28.0$ K. The Lorentz–Berthelot mixing rules were used to calculate the crossed parameters σ_{fw} and ε_{fw}. Modelling the multi-walled carbon nanotubes as structureless cylindrical walls is expected to be a good approximation since the diameter of the LJ CCl_4

(0.514 nm) is much larger than the C–C bond length in the carbon nanotubes (0.14 nm), and therefore the effect of surface corrugation is expected to be relatively small. A previous simulation work on freezing/melting of LJ methane confined within graphitic slit pores [3] showed quantitatively similar results for both smooth and structured graphite walls.

In this work we used the parallel tempering scheme in the grand canonical ensemble, as proposed by Yan and de Pablo [38]. In this method, a Monte Carlo (MC) simulation is performed simultaneously in n non-interacting replicas with volume V, each one at a different set of temperature T and chemical potential μ values. Standard grand canonical Monte Carlo (GCMC) trial moves are attempted at random with equal probability in each one of the replicas. In addition, configuration swaps are randomly proposed between pairs of replicas, subject to specific acceptance criteria [38]. These swap moves provide an effective way to deal with high energy barriers and metastability problems, considerably improving the sampling of phase space [38]. Parallel tempering schemes have been used in the past to study phase changes in 38-atom LJ clusters [39], specifically solid–liquid and solid–solid transitions involving icosahedral and fcc octahedral forms. The parallel tempering method has also been used recently to study the thermal stability of solid-like and liquid-like phases of C_{60} clusters [40], as well as the phase changes of the water octamer from very low temperatures up to the melting region [41].

A cylindrical simulation box with a pore diameter of $D = 5$ nm (corresponding to $D^* = D/\sigma_{ff} = 9.7$) was considered, and periodic boundary conditions were used at both ends. The reduced cylindrical pore length $L^* = L/\sigma_{ff}$ was fixed at $L^* = 60$. This pore length was chosen to get an appropriate L/D ratio. Previous simulations of freezing of LJ CCl_4 confined in graphitic slit-like pores have shown that for system sizes with $L^* \geqslant 60$ the results are self-consistent, meaning that fluctuations do not destroy the ordered phases observed in the simulations [21, 22]. Cell lists [42] were used to speed up the simulation runs, and typical systems had up to 4000 particles. For most runs, thermodynamic properties were averaged over 400 million MC steps. Longer runs were performed near the transition temperatures.

In our simulation runs we followed previous works [3, 6] in choosing sets of temperature and chemical potential such that the value of μ corresponded to the coexistence pressure. Such a path implies that the confined phase is always in equilibrium with a saturated vapour in the bulk. The properties of the LJ fluid at coexistence were obtained from [43]. We also followed the methodology of previous works [6] in measuring bond order parameters that were sensitive to the degree of crystallinity in the system. Three-dimensional (3D) bond orientational order parameters can be defined as follows [44, 45]:

$$Q_l = \left[\frac{4\pi}{2l+1} \sum_{m=-l}^{l} |\overline{Q}_{lm}|^2 \right]^{1/2}, \tag{2}$$

$$W_l = \frac{1}{\left(\sum_{m=-l}^{l} |\overline{Q}_{lm}|^2 \right)^{3/2}} \times \sum_{m_1, m_2 = -l}^{l} \begin{pmatrix} l & l & l \\ m_1 & m_2 & -m_1 - m_2 \end{pmatrix} \overline{Q}_{lm_1} \overline{Q}_{lm_2} \overline{Q}_{l(-m_1-m_2)}, \tag{3}$$

$$\overline{Q}_{lm} = \frac{1}{N_b} \sum_{i=1}^{N_b} Y_{lm}(\theta_i, \phi_i), \tag{4}$$

where N_b is the number of nearest neighbour bonds, Y_{lm} are the spherical harmonics [45] and the matrix in equation (3) is a representation of the Wigner $3J$ symbols [46]. Values of the 3D bond orientational order parameters for some common crystals are presented in table 1.

Significant ordering into distinct concentric molecular layers was found in the simulations. A representative quasi-two-dimensional configuration of the molecules within a layer j can be obtained by cutting the layer along the axial direction z and unrolling it flat. To study the layer freezing behaviour, two-dimensional (2D) bond orientational order parameters Φ_j were measured within each layer j [21, 47]:

$$\Phi_j = \frac{\left| \int \Psi_{6,j}(\mathbf{r}) \mathrm{d}\mathbf{r} \right|}{\int \mathrm{d}\mathbf{r}} \tag{5}$$

$$\Psi_{6,j}(\mathbf{r}) = \frac{1}{N_b} \sum_{k=1}^{N_b} \exp(i6\theta_k), \tag{6}$$

where $\Psi_{6,j}(\mathbf{r})$ measures the hexagonal crystalline bond order at a position $\mathbf{r}$ within layer j. We expect $\Phi_j = 1$ when the layer has the structure of a perfect, two-dimensional hexagonal crystal and $\Phi_j = 0$ when the layer

Table 1. Values of the three-dimensional bond orientational order parameters for some common crystals. From [6].

Crystal	Q_6	Q_4	W_6	W_4	$Q = Q_6 - 3W_4$
fcc	0.571	0.191	−0.013	−0.159	1.052
hcp	0.485	0.097	−0.012	0.134	0.082
bcc	0.511	0.036	0.013	0.159	0.033
sc	0.354	0.764	0.013	0.159	−0.124
icosahedral	0.663	0	−0.170	0	0.663
Liquid	0	0	0	0	0

has a two-dimensional isotropic structure. We also monitored the two-dimensional, in-plane positional and orientational pair correlation functions within each layer. The positional pair correlation function in layer j is given by the familiar radial distribution function $g_j(r)$ measured within the 2D plane formed by each unwrapped layer j, r being the in-layer distance. The orientational pair correlation function is given by [19]:

$$G_{6,j}(r) = \left\langle \Psi_j^*(0)\Psi_j(r) \right\rangle. \quad (7)$$

3. Results

3.1. *Experiment*

The dielectric constant κ_r is a natural choice of order parameter to study freezing of dipolar fluids, since the orientational polarizability undergoes large changes between the liquid and solid phases. In figure 1 we present measurements of the capacitance C as a function of temperature T for nitrobenzene confined in multi-walled carbon nanotubes with average internal and external pore diameters of 5 nm and 10 nm, respectively. The signal shows a sharp increase at 5.7°C, which corresponds to bulk melting. Two smaller and more rounded increases of C are present at 1°C and 8.5°C. For $T > 8.5$°C, the capacitance shows an incipient scaling with the inverse of temperature ($1/T$), which is typical for liquids, and indicates that all the nitrobenzene present in the system exists as liquid. These transition temperatures are in agreement with those observed in our measurements using differential scanning calorimetry on the same system. An analysis of the relaxation times (figure 2) provides an interpretation for the features observed in figure 1 at 1°C.

The relaxation time as a function of temperature for nitrobenzene within carbon nanotubes is presented in figure 2. In the millisecond branch ($\tau \sim 10^{-3}$ s), the signal corresponding to $T < 5.7$°C represents the dynamics of crystals of nitrobenzene either in the bulk or in the pore, whereas that at $T > 5.7$°C can be attributed to the Maxwell–Wagner–Sillars (MWS) polarization. This is a relaxation mechanism due to interfacial polarization in heterogeneous systems, which is known to have relaxation times of the order of 10^{-3} s [17]. The signal with $\tau \sim 10^{-7}$ s for $T > 5.7$°C is too slow to represent liquid nitrobenzene in the bulk, which is known to have relaxation times in the order of nanoseconds [17] and is out of the range of our measurements. Therefore this signal must represent the dynamics of liquid nitrobenzene within the pores. This branch disappears at 1°C, indicating that nitrobenzene no longer exists as liquid in the system (bulk + pores). Since the bulk melting temperature is 5.7°C, the melting temperature of nitrobenzene in the pores can be taken to be 1°C. The branch with relaxation times on the order of microseconds ($\tau \sim 10^{-6}$ s) exists for $T < 8.5$°C and indicates the presence of either highly defective micro-crystals or

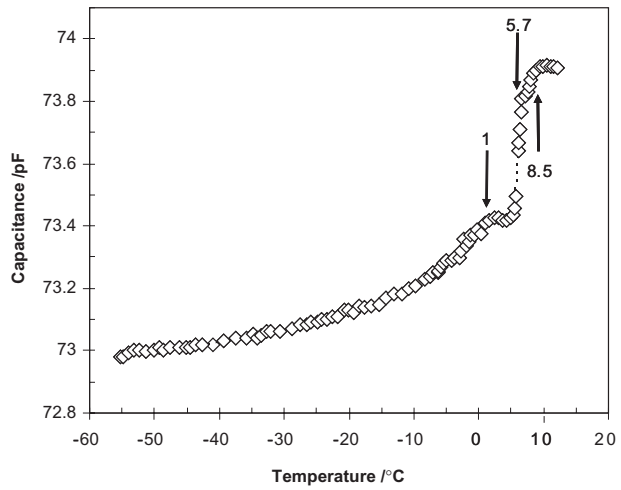

Figure 1. Capacitance C as a function of temperature T for nitrobenzene in multi-walled carbon nanotubes with average internal and external pore diameters of 5 nm and 10 nm, respectively. The measurements were performed at a frequency ω equal to 600 kHz. The signals are for both bulk and confined nitrobenzene, since the sample consisted of a suspension of carbon nanotubes in bulk nitrobenzene.

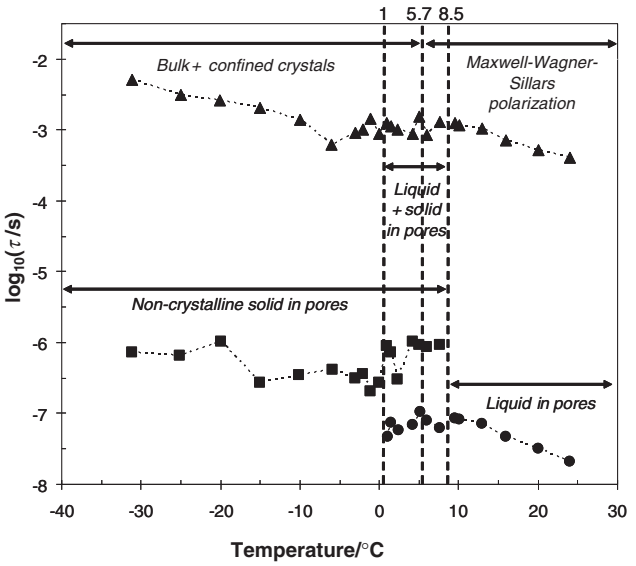

Figure 2. Relaxation time τ as a function of temperature T for nitrobenzene in multi-walled carbon nanotubes with average internal and external pore diameters of 5 nm and 10 nm, respectively. Three signals were observed during the experiments, with τ in the range of 10^{-3} s (triangles), 10^{-6} s (squares) and 10^{-7} s (circles). The signals are for both bulk and confined nitrobenzene, since the sample consisted of a suspension of carbon nanotubes in bulk nitrobenzene.

amorphous, glassy solids. Our results strongly suggest that the confined phase is inhomogeneous for temperatures between 1°C and 8.5°C, and liquid, crystalline and non-crystalline regions may coexist. For $T < 1$°C, the confined solid phase could be inhomogeneous and may consist of crystalline and non-crystalline nitrobenzene. Finally, only liquid nitrobenzene is present within the pores at $T > 8.5$°C. The exact structure of the confined phase cannot be determined from dielectric relaxation spectroscopy experiments alone; this information could be obtained from experimental techniques such as X-ray diffraction and neutron scattering, or from molecular simulations. The inhomogeneous nature of the confined phase at low temperatures can be attributed to the degree of confinement within a nanotube of $D = 5$ nm, which constrains the formation of a homogeneous, crystalline adsorbed phase. These results are in agreement with previous experimental studies of nitrobenzene in silica pores with similar diameters [17]. Inhomogeneities in the confined phase were also observed in previous molecular simulation studies of freezing within cylindrical pores [4, 13, 17], as well as in the simulations of CCl_4 within carbon nanotubes presented in this study.

In figure 3, the capacitance is shown as a function of temperature for CCl_4 confined within carbon nanotubes at different values of ω (30, 100 and 600 kHz). The features are qualitatively similar to those observed for nitrobenzene (figure 1). As in the nitrobenzene study, the sample was introduced between the capacitor plates as a suspension of CCl_4-filled carbon nanotubes in pure

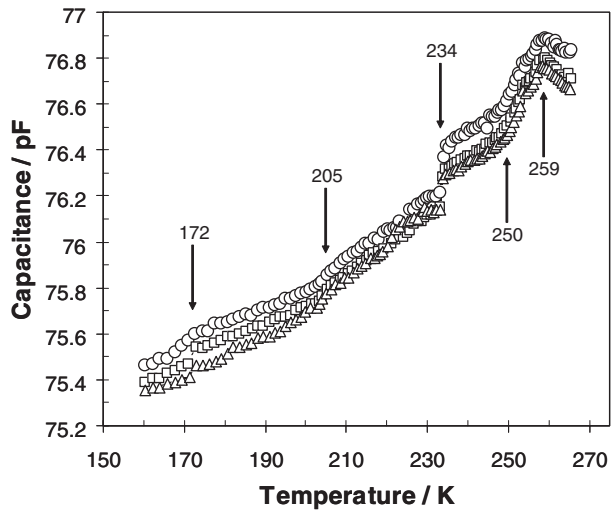

Figure 3. Capacitance C as a function of temperature T for carbon tetrachloride in multi-walled carbon nanotubes with average internal and external pore diameters of 5 nm and 10 nm, respectively. The measurements were performed at frequencies ω equal to 30 kHz (circles), 100 kHz (squares) and 600 kHz (triangles).

CCl_4; the volume of bulk CCl_4 in the sample was, however, very small, so that the signals represent mostly the confined adsorbate. The features found in the curves at 172 K may be associated with a solid–solid transition within the pore, since bulk CCl_4 undergoes a transition between the monoclinic and rhombohedric crystalline forms at 210 K. At 205 K there is a subtle change of slope in all the curves, suggesting that structural changes start to occur in the confined phase. These changes take place continuously up to 234 K, where there is a sharp increase in C. The capacitance scales with the inverse of the temperature $(1/T)$ at temperatures greater than 259 K, which is a clear sign that all the CCl_4 present in the system is liquid. As a result, the feature observed in the capacitance at 234 K may be associated to partial melting within the pore. The bulk melting point is reached at 250 K, where there are small changes in the slope of all the curves. This subtle response is mainly due to the small amount of CCl_4 in the bulk phase and its non-polar nature. Summarizing, one part of the CCl_4 in confinement melts between 205 K and 234 K, with the rest melting at 259 K; bulk CCl_4 in the sample melts at 250 K.

Measurements of the relaxation times for CCl_4 were not attempted. The relaxation times for CCl_4 are considerably faster than those for nitrobenzene, and thus only slow-dynamics processes such as MWS polarization and crystal relaxation will be detected. Moreover, the non-polar nature of CCl_4 produces weak signals in the experiments since the relaxations are mostly due to induced polarization (with frequencies in the range of GHz), rather than orientational polarizability effects, as is the case for polar fluids such as nitrobenzene. Further experiments with different techniques are needed to corroborate our observations, especially for the case of CCl_4, where relaxation times could not be determined. Differential scanning calorimetry experiments should corroborate the transition temperatures found by dielectric relaxation spectroscopy, while techniques such as X-ray diffraction and neutron scattering might allow us to determine the structure of the adsorbed phase. On the other hand, this information can be readily obtained from molecular simulations. Comparisons between experiments and simulations can provide some insight and help in the analysis of the results obtained.

3.2. *Simulation*

In our simulations using the parallel tempering Monte Carlo scheme, we started from well-equilibrated liquid-like and solid-like configurations obtained from previous, long GCMC runs (up to 10^{10} MC steps) at different temperatures. Then, we assigned these configurations randomly to each set of (T, μ), letting the

systems equilibrate. In our calculations with the parallel tempering Monte Carlo scheme, we have used as many as 50 different replicas in a single run, in order to cover all the phase space of interest and guarantee frequent swaps between replicas. The evolution of the parallel tempering simulation as a function of the number of Monte Carlo steps was monitored and, after equilibration, it was verified that each configuration visited many sets of (T, μ) along a single simulation run. The acceptance ratio for exchanging configurations was not completely uniform between all the replicas, meaning that the selected conditions of (T, μ) were not optimal and could be further refined. Nevertheless, the fraction of accepted swap moves was over 15% for all the replicas, which is considered satisfactory for a parallel tempering simulation [38, 48, 49].

The amount of CCl_4 adsorbed within a carbon nanotube is represented as a function of the temperature in figure 4(*a*). Figure 4(*b*) shows the average values of the three-dimensional bond order parameters Q_6 and Q_4 as a function of temperature. At relatively high temperatures ($T > 260$ K), the amount adsorbed gradually increases as the temperature decreases. The three curves exhibit jumps around 250–260 K and at 210–220 K. Further reduction in the temperature produces slight increases in the three variables, and GCMC simulations at $T = 177$ K suggest that negligible changes occur at temperatures lower than 192 K. Similar features were found for the 3D order parameters W_6, W_4 and Q. Jumps in the adsorption curve and 3D order parameters at 250–260 K and 210–220 K suggest that changes in the adsorbate structure take place at these temperature ranges. At the lowest temperature considered in the parallel tempering simulations ($T = 192$ K), the average values of the 3D order parameters were $Q_6 = 0.137$, $Q_4 = 0.044$, $W_6 = -0.095$, $W_4 = 0.125$ and $Q = -0.238$. A comparison of these values with those reported in table 1 suggests that the confined fluid does not solidify into any of the crystalline lattice structures presented in table 1; rather, the adsorbate forms five concentric layers within the pore, as can be seen from the density profile within the pore across the radial direction (figure 5). This finding is in agreement with previous simulation [4, 13, 17] and experimental [17, 50–52] studies, where it was shown that for silica materials with pore diameters below $20\sigma_{ff}$ only partial crystallization occurs. For silica materials, it was found [17, 50–52] that $D = 12\sigma_{ff}$ was the lower limit below which there are no 3D crystal domains in the system. Our results are also in excellent agreement with recent simulations performed by Hoffmann and Nielaba [31], who studied freezing of argon and neon within cylindrical pores of similar diameters using classical and path integral Monte Carlo simulations in the canonical (NVT) ensemble. For strongly attractive pores, the adsorbate was found to freeze in concentric layers, with the contact layer freezing at temperatures higher than the rest of the system. Structures with local fcc or hcp order were observed for pores with weak fluid–wall interactions. Nevertheless, further

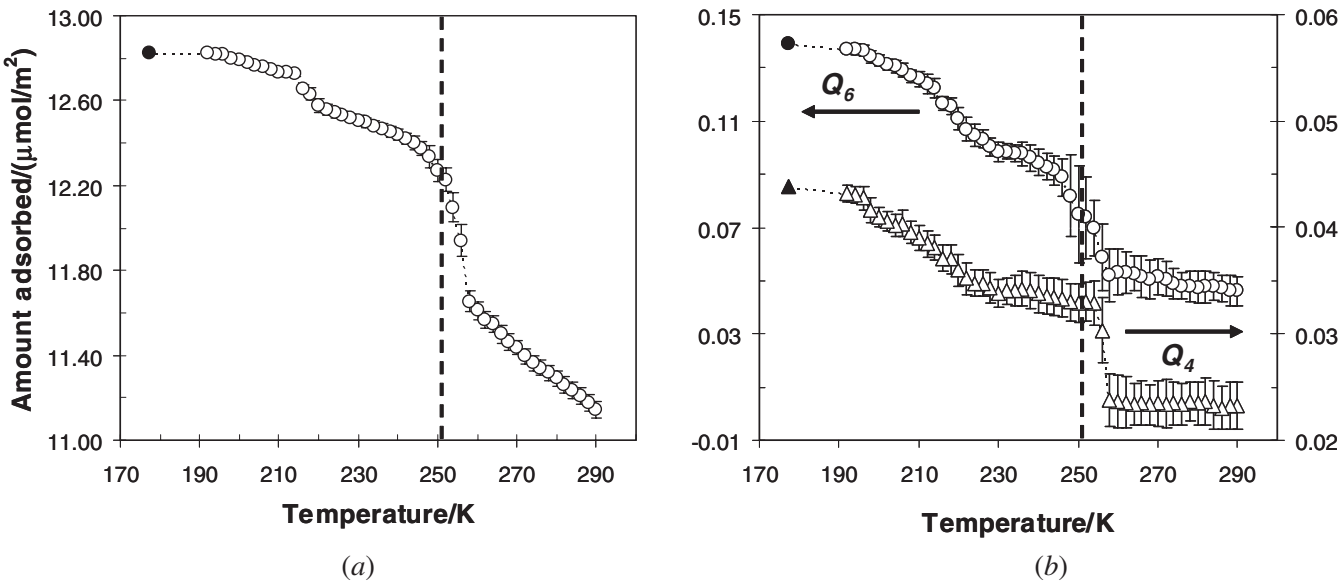

Figure 4. (*a*) Amount adsorbed, and (*b*) average values of the three-dimensional, bond orientational order parameters Q_6 (circles) and Q_4 (triangles), as a function of temperature for LJ CCl_4 confined in a model structureless, multi-walled carbon nanotube with $D^* = 9.7$ and $L^* = 60$, from parallel tempering simulations. The black filled symbols represent results from a GCMC simulation performed at $T = 177$ K. The thick dashed line represents the bulk solid–fluid phase transition temperature and the thin dashed lines between the symbols are provided as a guide to the eye.

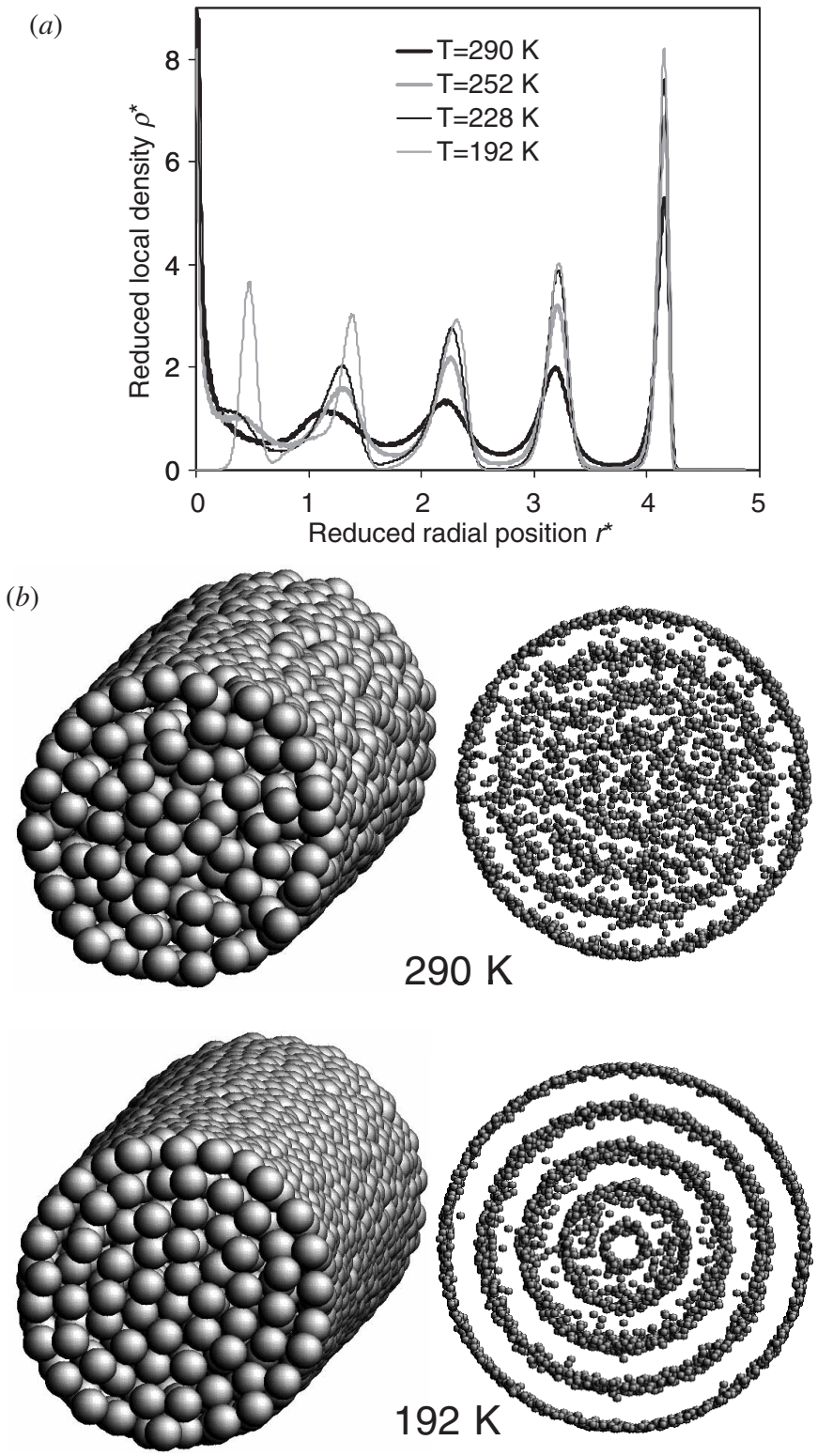

Figure 5. (*a*) Density profile along the radial direction at different temperatures for LJ CCl_4 confined in a structureless, multi-walled carbon nanotube with $D^* = 9.7$ and $L^* = 60$ at different temperatures: $T = 290$ K (thick black line), $T = 252$ K (thick grey line), $T = 228$ K (thin black line) and $T = 192$ K (thin grey line); (b) snapshots of typical configurations of the adsorbed phase at the highest ($T = 290$ K) and lowest ($T = 192$ K) temperatures considered. Front views of the same snapshots depicting only the centers of mass of the adsorbed CCl_4 molecules are also provided, to help visualize the formation of concentric layers as the temperature is reduced.

experimental investigation is needed to corroborate that, for the particular pore size used in this study, the confined CCl_4 does not solidify into any of the crystalline structures presented in table 1. Experimental techniques such as X-ray diffraction and neutron scattering could allow us to determine the structure of the adsorbate at different temperatures and confirm our observations.

In figure 5(a), the density profile of the adsorbed phase along the radial direction is presented at several temperatures. All the profiles show five peaks. The maxima in each peak increase and the inter-peak minima decrease as the temperature is reduced, indicating a well-defined layer separation. The snapshots presented in figure 5(*b*) corroborate this observation. The curves at $T = 290$ K, 252 K and 228 K show a steep rise near $r^* = 0$ and a shoulder around $r^* = 0.5$. In contrast, the profile at $T = 192$ K exhibits a zero value at $r^* = 0$ and a peak around $r^* = 0.5$. These features indicate that in most of the temperature range considered, the innermost region of the pore consists of a disordered array of molecules that finally arrange themselves into a concentric layer at relatively low temperatures (around $T = 196$ K). This effect is due to the high degree of confinement experienced by the molecules in the inner regions of the pore.

The average values of the two-dimensional bond order parameter in each layer as a function of temperature are presented in figure 6. The behaviour in the contact and second layers is very similar, both exhibiting a steep increase in their order parameter value around 250–260 K. This feature suggests that both molecular layers undergo a transition from an isotropic liquid to an ordered phase within this temperature range, which is slightly higher than the bulk freezing point of our LJ CCl_4 model (251 K). Further reductions

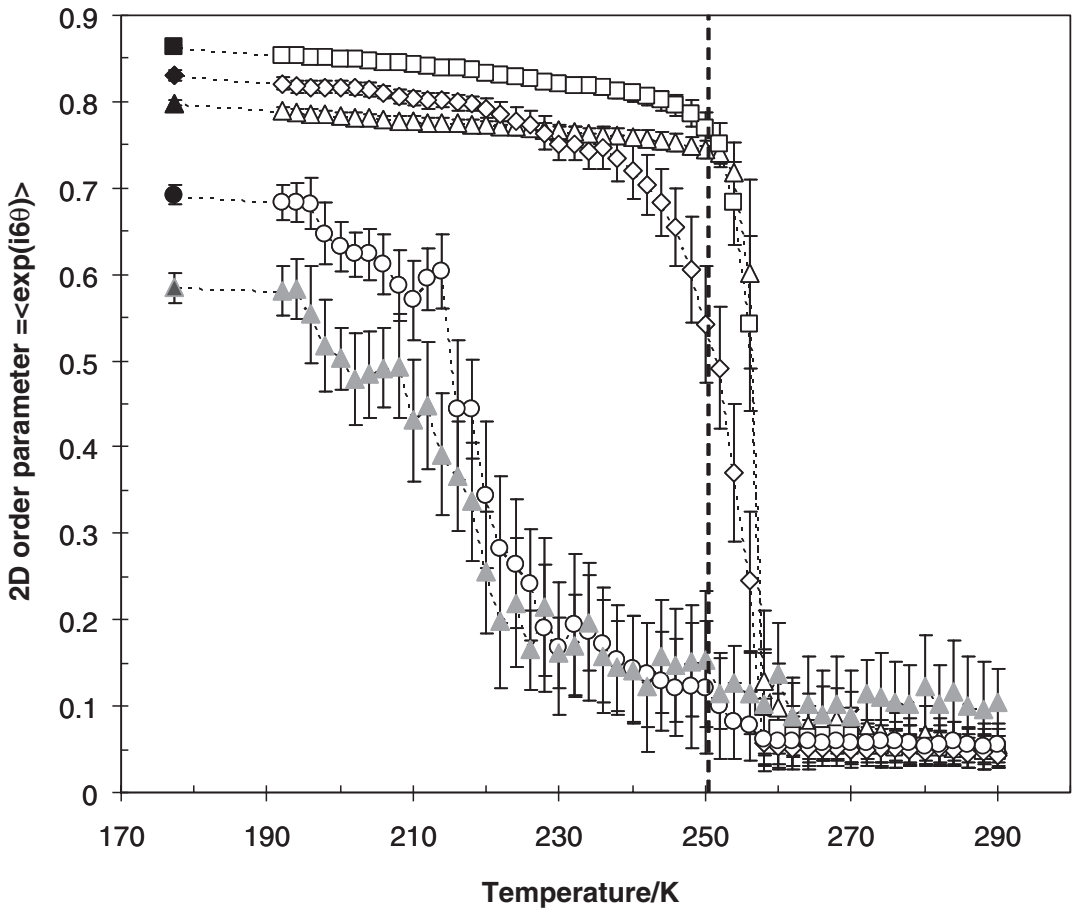

Figure 6. Average values of the two-dimensional bond orientational order parameter in the distinct fluid layers of LJ CCl_4 confined in a structureless, multi-walled carbon nanotube with $D^* = 9.7$ and $L^* = 60$, as a function of temperature. Open triangles, squares, diamonds, circles and grey triangles represent values for the contact, second, third, fourth and innermost layers, respectively, as obtained from parallel tempering simulations. The black filled symbols represent results from a GCMC simulation performed at $T = 177$ K. The thick dashed line represents the bulk solid–fluid phase transition temperature. The thin dashed lines between the symbols are provided as a guide to the eye.

of the temperature produce only small increases in the average order parameter value of these layers, which is not equal to 1 due to the presence of defects in the quasi-two-dimensional hexagonal crystals formed. In the third layer, the change in the order parameter is more gradual than in the first two layers and occurs in a wider temperature range, between 260 K and about 220 K. The fourth and the innermost layer show similar behaviour, with gradual increases in the order parameters values between 260 K and 230 K followed by a quick rise between 230 K and 210 K. At lower temperatures, the order parameters in the inner layers increase at a slower pace until they reach their maximum values, $\Phi \sim 0.7$ for the fourth layer and $\Phi \sim 0.6$ for the innermost layer. These values are relatively low when compared to those of the contact, second and third layers in their ordered phases, and suggest that the inner layers solidify into quasi-two-dimensional, highly defective micro-crystals. These results are in agreement with previous simulation studies [4, 13, 17]. The exact transition points between the phases present in the system can be determined by means of free energy calculations, which are currently being performed. The difference in the temperature ranges at which each layer undergoes a transition from an isotropic phase to an ordered structure can be explained in terms of the attractive interactions and the degree of confinement. Strongly attractive walls lead to increases in the adsorbate transition temperatures, and geometrical constraints produce depressions in the transition temperatures. The contact layer experiences a strong attraction from the pore wall, and the combined interaction of the pore wall and a tightly packed contact layer acts upon the second layer. Consequently, these two layers undergo a transition at temperatures slightly higher than the bulk freezing point. In contrast, the fourth and innermost layers experience a weaker effect from the attractive wall potential and are the most geometrically constrained, experiencing a high degree of confinement. Therefore, the transition to solid occurs at temperatures well below the bulk freezing point, and the ordered phase formed presents a large number of defects. Finally, the third layer undergoes a transition at intermediate temperatures, since its geometrical constraint is not as severe as that of the inner regions and the effect of the pore walls is weaker than in the outer layers.

Results for the in-plane positional and bond orientational pair correlation functions for the first four molecular layers at four different temperatures are presented in figure 7. Correlations in each layer were measured up to a distance $l = \pi r_l$, where r_l is the radial position where the reduced local density ρ^* reaches a maximum in each layer (figure 5(*a*)). Results for the innermost layer were not included since correlations in this layer could be measured up to a distance of only $1.6\sigma_{ff}$. At $T = 260$ K, all the layers exhibit an isotropic structure in the positional pair correlation function $g(r)$ and an exponential decay in the bond orientational pair correlation function $G_6(r)$. Therefore, all the layers behave as dense, isotropic fluids with short-range positional order and short-range bond orientational order. Both the contact and second layers appear as two-dimensional hexagonal crystals with defects at $T = 254$ K. This can be concluded from the features observed in the $g(r)$ function: a large value on the first peak, a first minimum of zero and an incipient splitting in the second and third peaks. Moreover, the constant value of $G_6(r)$ in the two outer layers at large r is also a signature of ordered hexagonal phases. Meanwhile, the remaining layers keep their isotropic characteristics. At $T = 228$ K, the third layer exhibits the same crystalline features as the outer layers, while the inner layers are still liquid-like. Finally, all layers are quasi-crystalline at $T = 196$ K, although the fourth layer exhibits a smaller first peak in the $g(r)$ function (as compared to the outer layers) and a non-zero value in the first minimum of the same function. These features indicate the presence of a large number of defects in the inner layers.

We note that the simulations presented in this study suggest the possible presence of intermediate states between the 2D hexagonal crystal and the 2D liquid in all the layers. In figure 6, there is a wide range of temperatures where the average 2D order parameter in each layer takes intermediate values between those exhibited by a 2D liquid ($\Phi \sim 0.1$) and a 2D crystal: $\Phi \sim 0.8$ in the first three layers, $\Phi \sim 0.6$ in the inner layers. In addition, there are temperatures where some layers show extended correlations in $g(r)$, as compared to those exhibited by a 2D liquid, and an algebraic decay in $G_{6,f}(r)$ (e.g., the third layer at $T = 254$ K in figure 7). System size is a key variable in determining the existence of such intermediate phases [21, 22]. Simulations using carbon nanotubes with larger pore diameters are currently in progress.

The simulations for CCl_4 seem to be in general agreement with the experimental results presented in figure 3. For the inner layers, sharp increases in the 2D order parameter were observed between 210 K and 230 K. The inner regions of the pore suffer strong geometrical constraints and thus are mostly frustrated crystals. Therefore, the features found in the experiments between 205 K and 234 K can be associated with the melting in the inner layers, and at 234 K the inner regions of the pore are liquid-like. In the simulations, the outer layers experience a sharp increase in their 2D order parameter value between 250 K and 260 K; in the experiments, the adsorbed CCl_4 remaining as solid melts between 250 K and 259 K, in good agreement with the

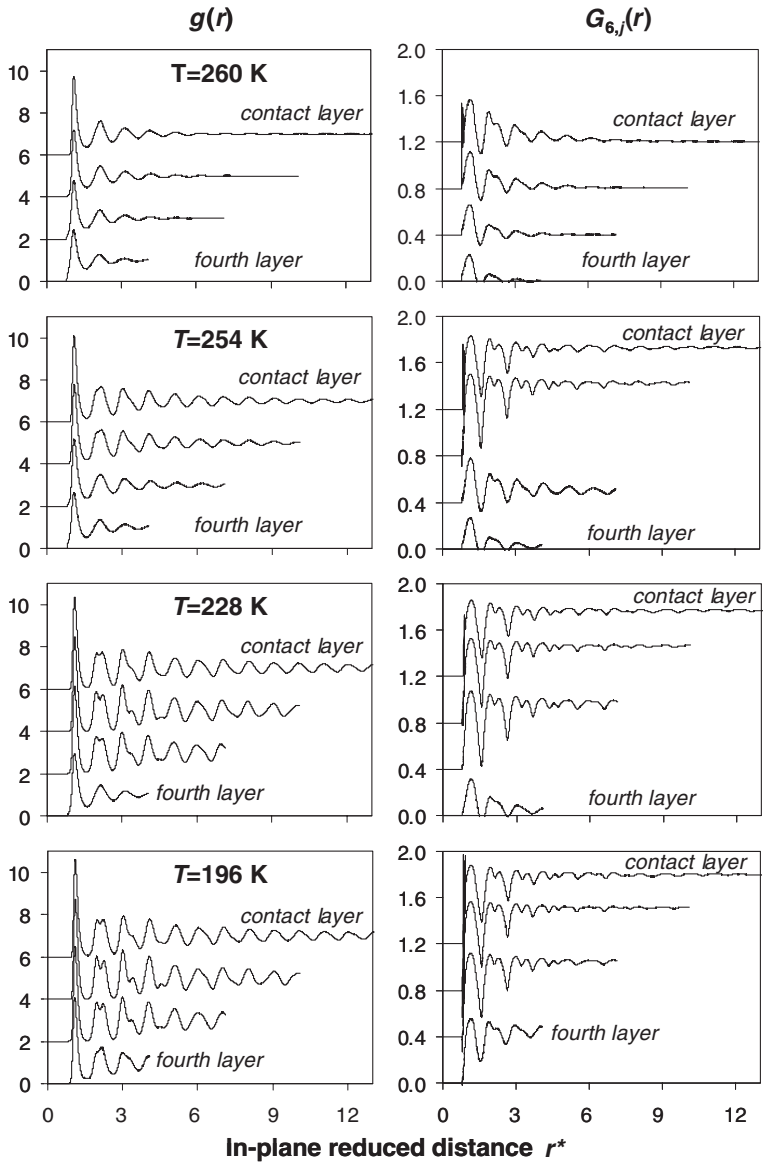

Figure 7. In-plane positional and bond orientational pair correlation functions for the first four molecular layers of LJ CCl_4 confined in a structureless, multi-walled carbon nanotube with $D^* = 9.7$ and $L^* = 60$, at four different temperatures. At $T = 260$ K, all layers are liquid-like. The contact and second layers are quasi-crystalline at $T = 254$ K, while the others layers remain liquid-like. At $T = 228$ K, the three outer layers are quasi-crystalline and the rest are liquid-like. Finally, all layers are quasi-crystalline at $T = 196$ K.

simulations. Moreover, in the simulations the third layer shows an intermediate behaviour between the outer and the inner regions, increasing its 2D order parameter value continuously between 260 K and 220 K. Such an intermediate behaviour can be taken to contribute to the features shown in the experiments in both the inner and outer regions. The features observed in the experiments at 172 K, which were associated with a possible solid–solid transition within the pores, were not observed in the simulations.

4. Conclusions

A combined experimental–simulation study of freezing in confinement within carbon nanotubes was presented. The simulations show that the adsorbate forms concentric layers that solidify into quasi-two-dimensional hexagonal crystals with defects. Owing to the strong geometrical constraints, the number of defects is particularly high for the inner layers, which form frustrated crystals. Our simulations show no formation of common 3D crystalline structures

(fcc, hcp, bcc, sc or icosahedral) in confinement. Both simulations and experiments suggest the presence of inhomogeneous phases (i.e., combinations of crystalline, liquid and frustrated crystalline regions) within the pore, over extended temperature ranges. In particular, 'contact layer' phases were observed, in which the adsorbate close to the pore wall has a different structure from that in the interior of the pore. Our results indicate that the outer layers of adsorbate solidify at temperatures slightly higher than the bulk freezing point, whereas the inner layers experience a depression in the transition temperature with respect to the bulk. The simulation results are in general agreement with the experimental measurements. Further experiments with different techniques are needed to corroborate our observations. Differential scanning calorimetry experiments should corroborate the measured transition temperatures, while techniques such as X-ray diffraction and neutron scattering might allow us to determine the structure of the adsorbed phase. Simulations of nitrobenzene within carbon nanotubes are currently in progress, as well as simulations using pores of larger diameters. The formation of confined 3D crystalline structures should not be hindered in such larger pores [17, 50–52], and the occurrence of intermediate phases during the freezing process might be determined. We are also performing free energy calculations to determine the thermodynamic transition temperatures between the different phases present in the system. Although the use of the parallel tempering technique in simulations greatly reduces the probability of getting trapped in a metastable state, a free energy calculation will allow us to determine the thermodynamic stability of each of the phases present in the system in a rigorous way.

F. R. H. is grateful to Henry Bock, Coray Colina, Benoit Coasne and Erik Santiso (North Carolina State University), Jorge Pikunic (University of Oxford, UK), Ravi Radhakrishnan (New York University) and Flor Siperstein (Universitat Rovira I Virgili, Spain) for helpful discussions. It is a pleasure to thank François Beguin and his group at CNRS-Orléans, who synthesized the carbon nanotubes used in the experiments. This work was supported by grants from the National Science Foundation (grant no. CTS-0211792), the Committee of Scientific Research of Poland (grant KBN no. 2P03B 014 24) and an Adam Mickiewicz University Rector Grant (2003). International cooperation was supported by a NATO Collaborative Linkage Grant (No. PST.CLG.978802). Supercomputer time was provided by the National Partnership for Advanced Computational Infrastructure (NSF/NRAC grant MCA93SO11) and the National Energy Research Scientific Computing Center (DOE grant no. DE-FGO2-98ER14847).

References

[1] Gelb, L. D., Gubbins, K. E., Radhakrishnan, R., and Sliwinska-Bartkowiak, M., 1999, *Rep. Prog. Phys.*, **62,** 1573.
[2] Christenson, H. K., 2001, *J. Phys.: condens. Matter.*, **13,** R95.
[3] Miyahara, M., and Gubbins, K. E., 1997, *J. chem. Phys.*, **106,** 2865.
[4] Maddox, M. W., and Gubbins, K. E., 1997, *J. chem. Phys.*, **107,** 9659.
[5] Dominguez, H., Allen, M. P., and Evans, R., 1999, *Molec. Phys.*, **96,** 209.
[6] Radhakrishnan, R., and Gubbins, K. E., 1999, *Molec. Phys.*, **96,** 1249.
[7] Sliwinska-Bartkowiak, M., Gras, J., Sikorski, R., Radhakrishnan, R., Gelb, L. D., and Gubbins, K. E., 1999, *Langmuir*, **15,** 6060.
[8] Kaneko, K., Watanabe, A., Iiyama, T., Radhakrishnan, R., and Gubbins, K. E., 1999, *J. phys. Chem.* B., **103,** 7061.
[9] Duffy, J. A., and Alam, M. A., 2000, *Langmuir*, **16,** 9513.
[10] Morishige, K., and Kawano, K., 2000, *J. chem. Phys.*, **112,** 11 023.
[11] Morishige, K., and Kawano, K., 2000, *J. phys. Chem.* B., **104,** 2894.
[12] Radhakrishnan, R., Gubbins, K. E., and Sliwinska-Bartkowiak, M., 2000, *J. chem. Phys.*, **112,** 11 048.
[13] Kanda, H., Miyahara, M., and Higashitani, K., 2000, *Langmuir*, **16,** 8529.
[14] Morishige, K., and Ogisu, Y., 2001, *J. chem. Phys.*, **114,** 7166.
[15] Qiao, Y., and Christenson, H. K., 2001, *Phys. Rev. Lett.*, **86,** 3807.
[16] Schreiber, A., Ketelsen, I., and Findenegg, G. H., 2001, *Phys. Chem. chem. Phys.*, **3,** 1185.
[17] Sliwinska-Bartkowiak, M., Dudziak, G., Sikorski, R., Gras, R., Radhakrishnan, R., and Gubbins, K. E., 2001, *J. chem. Phys.*, **114,** 950.
[18] Koga, K., Gao, G. T., Tanaka, H., and Zeng, X. C., 2001, *Nature*, **412,** 802.
[19] Ghatak, C., and Ayappa, K. G., 2001, *Phys. Rev.* E., **64,** 051 507.
[20] Kegel, W. K., 2001, *J. chem. Phys.*, **115,** 6538.
[21] Radhakrishnan, R., Gubbins, K. E., and Sliwinska-Bartkowiak, M., 2002, *J. chem. Phys.*, **116,** 1147.
[22] Radhakrishnan, R., Gubbins, K. E., and Sliwinska-Bartkowiak, M., 2002, *Phys. Rev. Lett.*, **89,** 076 101.
[23] Ayappa, K. G., and Ghatak, C., 2002, *J. chem. Phys.*, **117,** 5373.
[24] Denoyel, R., and Pellenq, R. J. M., 2002, *Langmuir*, **18,** 2710.
[25] Gedat, E., Schreiber, A., Albrecht, J., Emmler, T., Shenderovich, I., Findenegg, G. H., Limbach, H.-H., and Buntkowsky, G., 2002, *J. phys. Chem.* B., **106,** 1977.
[26] Miyahara, M., Sakamoto, M., Kanda, H., and Higashitani, K., 2002, *Stud. Surf. Sci. Catal.*, **144,** 411.
[27] Valiullin, R., and Furó, I., 2002, *J. chem. Phys.*, **117,** 2307.

[28] Morishige, K., and Iwasaki, H., 2003, *Langmuir*, **19,** 2808.
[29] Patrykiejew, A., Salamacha, L., and Sokolowski, S., 2003, *J. chem. Phys.*, **118,** 1891.
[30] Vishnyakov, A., and Neimark, A. V., 2003, *J. chem. Phys.*, **118,** 7585.
[31] Hoffmann, J., and Nielaba, P., 2003, *Phys. Rev.* E, **67,** 036 115.
[32] Delpeux, S., Szostak, K., Franckowiak, E., Bonnamy, S., and Beguin, F., 2002, *J. Nanosc. Nanotec.*, **2,** 481.
[33] Debye, P., 1929, *Polar Molecules* (New York: Chemical Catalog).
[34] Chelkowski, A., 1980, *Dielectric Physics* (New York: Elsevier).
[35] Peterson, B. K., Walton, J. P. R. B., and Gubbins, K. E., 1986, *J. chem. Soc., Faraday Trans. 2*, **82,** 1789.
[36] Steele, W. A., 1973, *Surf. Sci.*, **36,** 317.
[37] Steele, W. A., 1974, *The Interaction of Gases with Solid Surfaces* (Oxford: Pergamon Press).
[38] Yan, Q., and de Pablo, J. J., 1999, *J. chem. Phys.*, **111,** 9509.
[39] Neirotti, J. P., Calvo, F., Freeman, D. L., and Doll, J. D., 2000, *J. chem. Phys.*, **112,** 10 340; Calvo, F., Neirotti, J. P., Freeman, D. L., and Doll, J. D., 2000, *J. chem. Phys.*, **112,** 10 350.
[40] Calvo, F., 2001, *J. Phys. Chem.* B, **105,** 2183.
[41] Nigra, P., Carignano, M. A., and Kais, S., 2001, *J. chem. Phys.*, **115,** 2621.
[42] Frenkel, D., and Smit, B., 2002, *Understanding Molecular Simulation: From Algorithms to Applications*, 2nd Edition (London: Academic Press).
[43] Kofke, D. A., 1993, *J. chem. Phys.*, **98,** 4149; Agrawal, R., and Kofke, D. A., 1995, *Molec Phys.*, **85,** 43.
[44] Steinhardt, P. J., Nelson, D. R., and Ronchetti, M., 1983, *Phys. Rev.* B., **28,** 784.
[45] Gray, C. G., and Gubbins, K. E., 1984, *Theory of Molecular Liquids* (Oxford: Clarendon Press).
[46] Landau, L. D., and Lifshitz, E. M., 1965, *Quantum Mechanics* (New York: Pergamon Press).
[47] Mermin, N. D., 1968, *Phys. Rev.*, **176,** 250.
[48] Sugita, Y., Kitao, A., and Okamoto, Y., 2000, *J. chem. Phys.*, **113,** 6042.
[49] Faller, R., Yan, Q., and de Pablo, J. J., 2002, *J. chem. Phys.*, **116,** 5419.
[50] Morineau, D., Dosseh, G., Alba-Simionesco, C., and Llewellyn, P., 1999, *Philos. Mag.* B, **79,** 1847.
[51] Dosseh, G., Morineau, D., and Alba-Simionesco, C., 2000, *J. Phys.* IV, **10,** Pr7-99.
[52] Morineau, D., Casas, F., Alba-Simionesco, C., Grosman, A., Bellisent-Funel, M.-C., and Ratovélomanana, N., 2000, *J. Phys.* IV, **10,** Pr7-95.